Theses and Dissertations   1. Thesis and Dissertation Collection, all items

2019-06

NOVEL FORMULATIONS AND PROCESSING CONDITIONS TO 3D PRINT CU ALLOYS FOR NAVAL APPLICATIONS

Supe, Gabriel D.

Monterey, CA; Naval Postgraduate School

http://hdl.handle.net/10945/62798

NAVAL POSTGRADUATE SCHOOL

MONTEREY, CALIFORNIA

THESIS

NOVEL FORMULATIONS AND PROCESSING CONDITIONS TO 3D PRINT CU ALLOYS FOR NAVAL APPLICATIONS

by

Gabriel D. Supe

June 2019

Thesis Advisor: Claudia C. Luhrs
Second Reader: Garth V. Hobson

THIS PAGE INTENTIONALLY LEFT BLANK

REPORT DOCUMENTATION PAGE		*Form Approved OMB No. 0704-0188*

1. AGENCY USE ONLY *(Leave blank)*	2. REPORT DATE June 2019	3. REPORT TYPE AND DATES COVERED Master's thesis

4. TITLE AND SUBTITLE NOVEL FORMULATIONS AND PROCESSING CONDITIONS TO 3D PRINT CU ALLOYS FOR NAVAL APPLICATIONS	5. FUNDING NUMBERS
6. AUTHOR(S) Gabriel D. Supe	

7. PERFORMING ORGANIZATION NAME(S) AND ADDRESS(ES) Naval Postgraduate School Monterey, CA 93943-5000	8. PERFORMING ORGANIZATION REPORT NUMBER

9. SPONSORING / MONITORING AGENCY NAME(S) AND ADDRESS(ES) NRP	10. SPONSORING / MONITORING AGENCY REPORT NUMBER

11. SUPPLEMENTARY NOTES The views expressed in this thesis are those of the author and do not reflect the official policy or position of the Department of Defense or the U.S. Government.

12a. DISTRIBUTION / AVAILABILITY STATEMENT Approved for public release. Distribution is unlimited.	12b. DISTRIBUTION CODE A

13. ABSTRACT (maximum 200 words)

Research was conducted for the development of formulations for additive manufacturing of metal nanoparticles that produced a 3D printed metal object without oxidation but with material properties and corrosion resistance similar to existing approaches. The study was designed around experimentation of different liquids/viscous fluids that when mixed with metal nanoparticles, formulated a paste that can be used in extrusion 3D printers. A suitable binding agent, water/ethanol-based gel, was chosen to produce the initial paste to be 3D printed. The ideal printing conditions for the metal powder paste were found through trial and error. The pastes and products were analyzed and tested for oxidation and material properties using X-ray diffraction, electron microscopy, and nano mechanical testing. The study was limited to the use of copper alloys; for example, monel. The finished product was a metal design that retains the material properties of the desired metal and a Vickers hardness of 99.78. The porosity was able to be reduced to 10.56% in the sample after heat treatment.

14. SUBJECT TERMS extrusion printing, metal nano particles, electron microscopy, paste formulation, 3D printing, Cu alloys	15. NUMBER OF PAGES 71
	16. PRICE CODE

17. SECURITY CLASSIFICATION OF REPORT Unclassified	18. SECURITY CLASSIFICATION OF THIS PAGE Unclassified	19. SECURITY CLASSIFICATION OF ABSTRACT Unclassified	20. LIMITATION OF ABSTRACT UU

NSN 7540-01-280-5500

Standard Form 298 (Rev. 2-89)
Prescribed by ANSI Std. 239-18

THIS PAGE INTENTIONALLY LEFT BLANK

NOVEL FORMULATIONS AND PROCESSING CONDITIONS TO 3D PRINT CU ALLOYS FOR NAVAL APPLICATIONS

Gabriel D. Supe
Lieutenant, United States Navy
BS, U.S. Naval Academy, 2012

Submitted in partial fulfillment of the
requirements for the degree of

MASTER OF SCIENCE IN MECHANICAL ENGINEERING

from the

**NAVAL POSTGRADUATE SCHOOL
June 2019**

Approved by: Claudia C. Luhrs
Advisor

Garth V. Hobson
Second Reader

Garth V. Hobson
Chair, Department of Mechanical and Aerospace Engineering

THIS PAGE INTENTIONALLY LEFT BLANK

ABSTRACT

Research was conducted for the development of formulations for additive manufacturing of metal nanoparticles that produced a 3D printed metal object without oxidation but with material properties and corrosion resistance similar to existing approaches. The study was designed around experimentation of different liquids/viscous fluids that when mixed with metal nanoparticles formulated a paste that can be used in extrusion 3D printers. A suitable binding agent, water/ethanol-based gel, was chosen to produce the initial paste to be 3D printed. The ideal printing conditions for the metal powder paste were found through trial and error. The pastes and products were analyzed and tested for oxidation and material properties using X-ray diffraction, electron microscopy, and nano mechanical testing. The study was limited to the use of copper alloys; for example, monel. The finished product was a metal design that retains the material properties of the desired metal and a Vickers hardness of 99.78. The porosity was able to be reduced to 10.56% in the sample after heat treatment.

THIS PAGE INTENTIONALLY LEFT BLANK

TABLE OF CONTENTS

LIST OF FIGURES

LIST OF TABLES

THIS PAGE INTENTIONALLY LEFT BLANK

LIST OF ACRONYMS AND ABBREVIATIONS

AIP	American Isostatic Presses
AM	additive manufacturing
CuNi	copper nickel
BSD	backscattered electron detection
BSE	back scatter electron
DSC	differential scanning calorimetry
DoD	Department of Defense
EDS	electron dispersive X-ray spectroscopy
EHT	electric high-tension voltage
HIP	hot isostatic press
PBF	powder bed fusion
PSD	porosity size distribution
SE	secondary electrons
SEM	scanning electron microscope
STA	simultaneous thermal analysis
STL	stereo-lithography
TGA	thermogravimetry analysis
XRD	X-ray diffraction

THIS PAGE INTENTIONALLY LEFT BLANK

ACKNOWLEDGMENTS

First, I would like to thank the Naval Research Program for the opportunity to begin this research area and the funding the project. I would also like to thank the professors in the Mechanical Engineering Department, including Dr. Park, Dr. Ansel, and Dr. Menon, who helped me through various processes of preparing samples and the follow-on analysis. Thank you for taking the time to teach me and assist me in my work.

Lastly, I offer a very special thanks to Dr. Luhrs, my sole thesis advisor throughout the entire process. I've learned an incredible amount from you, and I could not have progressed as I have without you and your enthusiasm.

THIS PAGE INTENTIONALLY LEFT BLANK

I.   INTRODUCTION

A.   METAL POWDER IN ADDITIVE MANUFACTURING

Additive manufacturing is a prominent technology currently being explored and employed by industry and the U.S. military. Industries, including medical, automotive, and space systems, all use 3D printed technology. Computers, phones and even cars have been built using metal 3D printers with many other applications being researched. From building bridges to weapons, and even underwater vessels, the Department of Defense (DoD) has shifted its focus and money into the future of 3D printing. Of the proposed $639.1 billion budget, $13.2 billion has been set aside for 3D printing technologies [1].

Additive manufacturing has many benefits and applications for the U.S. military. The procurements of parts and cost are greatly reduced if they can be designed and created on site. The military would also save time from having to manufacture and ship desired parts. With the help of 3D scanners, a broken part can be scanned and loaded onto a 3D printer, which can then reproduce that part. Critical components of military equipment could be repaired on site and within hours or days instead of weeks or months.

The convenience of customizable parts is also a benefit because the parts can be tailored to meet specific needs. Composition of the powders can be changed to produce alloys with desired material characteristics, such as yield strength, malleability, corrosion resistance, and hardness. 3D printing also enables the user to change different aspects of the part, such as size and shape, when printing, which will enable users to improve on designs or redesign faulty parts. 3D metal printing will enable the United States to stay ahead of its adversaries and competitors by providing reliable, high strength parts to units forward deployed on site all while at reduced costs.

B.   BACKGROUND

Copper and nickel elements are next to each other on the periodic table with atomic weights of 63.5 5g/mol and 58.69 g/mol, respectively. Nickel is known for its hardness and ductility. It exists as an FCC crystal structure with electromagnetic properties and is considered a conductor. Copper is a soft and ductile metal with high electrical and thermal

conductivity. Copper exists in a solid phase as an FCC structure, which means when mixed together, copper and nickel will be completely soluble in liquid and solid states. When combined, copper and nickel can form many different CuNi alloys depending on the composition of copper and nickel. Other elements such as manganese, titanium, iron, and zinc can be added to the alloy to modify material properties of the alloy such as corrosion resistance, fatigue limits, and malleability.

Early uses of copper and nickel was found as far back at 250 BC when the Chinese created weapons from copper nickel alloys [2]. More recently, copper nickel alloys have been used by many countries for coins, such as the U.S. five cent coin because of its high resistance to wear and oxidation. Cupronickel was first used in naval applications by the British Navy in the 1920s for their naval condensers [3]. Once its corrosion resistant properties were discovered, the material began being used for a variety of marine applications including seawater pumps, piping, condensers, and the hulls of ships. CuNi alloys are still being applied today with new alloys such as Inconel and Monel, which continue to be improved upon.

Conventional methods of creating metal alloys consist primarily of powder metallurgy, casting, machining and metal injection molding. Metal powder bed fusion (PBF) is the current leading technology for metal 3D printing. The process involves using a laser or electron beam to heat and fuse metal powders together at extremely high temperatures. The parts are then transferred to heating oven to be sintered. The process is relatively slow, and the equipment is expensive to purchase and use due to high power costs. Finished samples also lack the similar material properties from cast metals as a result of the fusion process. Other issues include high surface roughness, impurities in the metal, high porosity, and residual stresses. Industry also continues to suffer from consistency and repeatability when attempting to scale production [4]. Deposition rates, porosity and density are different from sample to sample, making it difficult to replicate the same exact part repeatedly.

Binder Jetting is another method of Additive Manufacturing in which powder materials are combined with a binder which can be extruded though an inkjet deposition. This method enables parts to be printed without support structures or excess material. The

process works by extruding a binding material that attaches to the powder bed layer by layer. Then more powder is added, and the binding agent continues to be printed into a desired shape. Binder jetting printers can also print difficult shapes and structures, which are not possible through casting or machining. The binder jetting method can be used with polymers, ceramics, and metals.

The primary issues with binder jetting printing is the resulting high porosity and low density of the finished parts. Porosity reduces the strength and conductivity of a sample. The high porosity is a result of the binder being removed from the samples during heat treatment, leaving behind voids and micro-sized holes in the sample. Another downside of binder jetting is the shrinkage of the specimen during heat treatment as the binding agent is removed. Shrinkage as much as 77% has been observed for copper powder using binder jetting 3D printers [5].

Additive deposition is a relatively new technique for 3D printing in which powders are combined together with a binding material to create a paste, which can be extruded though a 3D printer. The paste is then printed layer by layer onto a base plate, requiring no support material. The adhesive properties of the binding agent, along with the surface tension and ideal viscosity of the mixture allow the paste to be printed and still hold its shape onto the base plate. Another advantage is not requiring heat to print which lowers production costs and minimizes safety issues. Samples produced through additive deposition are in their "green state" which means they are fragile and the powders have not yet fused together. This process in done for metals through sintering at high temperatures. The sintering process also removes the binding agent, which enables the metal particles to react and form an alloy with each other.

In order to reduce the porosity and increase the density of the parts, different temperatures and pressures were tested during the heat treatment process. Hot isostatic pressing (HIP) metal powders has shown to decrease porosity in samples [6] while increasing the density and fusing the powders together. Kumar also noted that increasing the density has resulted in higher yield strength and higher hardness [6]. This study examined the effects of HIP on 3D printed specimens and the resulting porosity size, distribution and size reduction of the samples.

3

C.   OBJECTIVES

The overarching goal of this research was to fabricate Cu-Ni metal alloy objects employing alternative 3D printing techniques using paste as starting material along low cost methods and equipment. Various printing methods were explored to achieve this goal, including diverse printing conditions and types of 3D printers. Different paste formulations were utilized to reduce porosity and improve the material characteristics of the samples such as hardness. The finished specimens needed to have a hardness comparable to other fabrication techniques for copper nickel alloys. Research by Zadi-Maad has found nickel-based alloys created with additive manufacturing are similar and even sometimes better than the conventional alloys [7].

The first objective was to test different binding agents and select the one that will enable the metal powders to be mixed together and extruded through a 3D printer nozzle. The binding agent selection was crucial to the sintering process because its removal directly affected porosity of the metal object being fabricated. Moreover, the binding agent needed to be removed from the sample during the post-treatment process to ensure the metal powders fused together without oxidation or other reactions occurring with the chemicals inside the binding material.

Previous work by Anantachaisilp found that the size and shape of NiTi particles affected the viscosity of the mixture being printed [8]. Adequate viscosity is required to control of the extrusion rate and speed of the printing. Thus, for this work, as a second objective, we determined the viscosity of pastes produced with different Cu and Ni particulate sizes under diverse shear rates using a rheometer.

A third objective of this research was to explore post-fabrication heat treatment methods, which would lower the porosity of the 3D printed metal while retaining the material properties and targeted composition. Thus, the last section of this thesis tested different sintering processes and temperature profiles to determine the optimal conditions to fabricate Cupronickel alloys. These processes required knowledge of the base metals and how they would react at different temperatures and compositions. Understanding the phases of copper and nickel was crucial to producing a successful alloy. Copper-nickel

alloys tend to absorb gases such as oxygen and hydrogen during the heat treatment process so an inert environment needed to be tested to prevent reaction of atmospheric gases [9].

The chapters of the thesis present the methods and materials employed to achieve the goals mentioned above, the results generated and a discussion regarding how the outcome compares with other fabrication approaches.

To conclude, the manuscript summarizes how, according to the data generated, paste 3D printing is a viable alternative to create copper nickel alloys. It is demonstrated that metal parts can be produced at low costs and minimal equipment while preserving the material properties of the alloys observed in other fabrication methods.

THIS PAGE INTENTIONALLY LEFT BLANK

II.   EXPERIMENTAL METHODS

This chapter introduces the methods used to create 3D printed alloys with copper and nickel paste. This chapter also discusses the various equipment used in the experiments and the settings required for each respective step of creation.
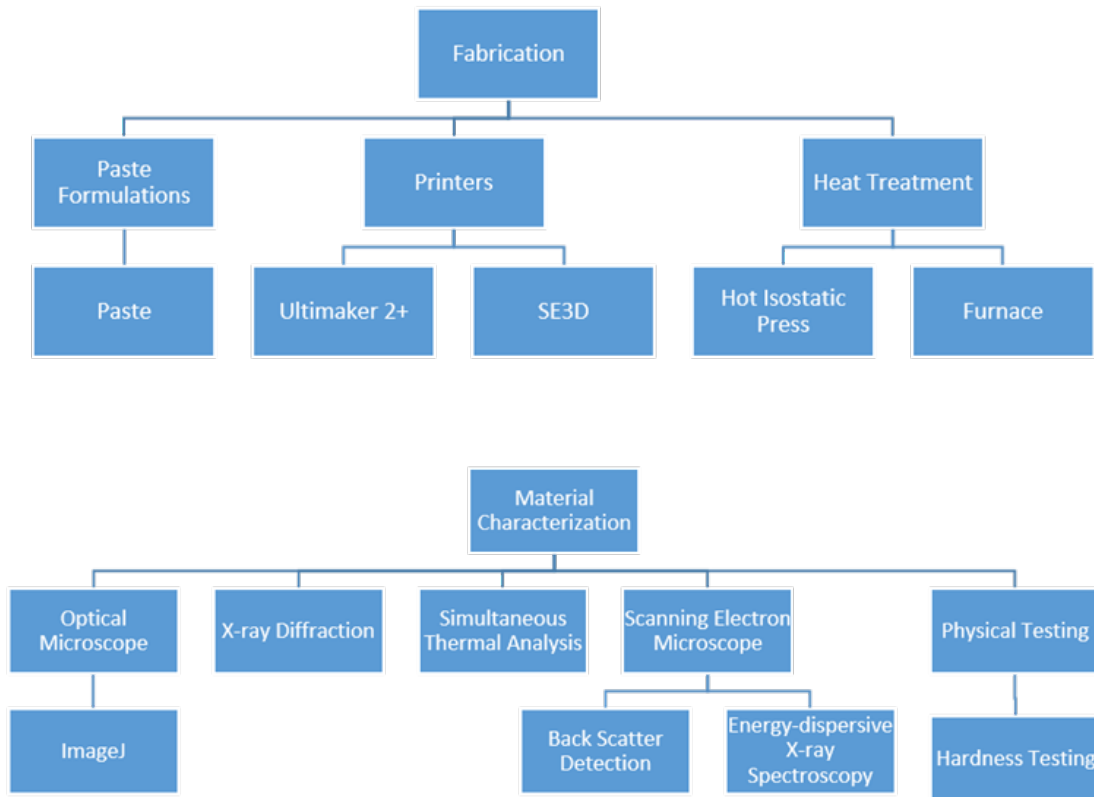
Figure 1.   Flowchart of Experimental Approach

A.   FABRICATION

This section discusses the unique 3D printing method used by additive deposition. Specific materials are used which enable this type of printing to be used in a 3D printer.

1.   Paste Formulations

The metal powders selected for this research were copper micron (Goodfellow, 5 micron, 99.8% purity), copper nanopowder (U.S. Research Nanomaterials Inc., 70nm particle size, 99.9% purity), nickel nano-powder (Sigma-Adrich, <100nm average particle size, >99% trace metal basis), and nickel micropowder (Sigma-Adrich, 5 micron average particle size, 99.7% trace metal basis). These metals were chosen due to their high corrosion resistance in seawater and high strength of the alloys, which are highly desired in naval applications. Copper/nickel alloys have been used extensively in shipbuilding applications such as hulls, seawater cooling systems, heat exchangers and piping due to the alloy's unique properties.

Copper micron and nano-powders were mixed with nickel micron and nano-powder. The finely mixed powders are able to be sintered together to form cupronickel (CuNi). Cupronickel has a high corrosion resistance and strong tensile strength, high ductility, and thermal conductivity. The metal powder mixture consisted of and even 50% copper and 50% nickel by percent weight. The atomic percent of the mixture is approximately 51.6% copper and 48.4% nickel.

a.   *Binding Agent*

Paste formulation for extrusion printing. In order to be able to utilize the 3D printers available, the metal powers needed to be mixed with a suitable binding agent. The resulting paste would then be placed into a syringe to be extruded by the printer and onto a printing bed for the paste to adhere to. The objective of the binding agent was to hold the power particles together for printing a specimen but leave no residue or oxidation after post-treatment processes. Previous work by Anantachaisilp has shown that alcohol-based gel can be used as a binding agent and contains desirable qualities for the sintering process [7].

Hydrocarbon saturated paraffin was tested as a possible binding agent with the metal powders. The paraffin is a mixture of saturated hydrocarbons with a melting point of 36°C and viscosity of 18.2 cSt at 100°C [10]. The other binding agent used was an alcohol-based gel made of 70% ethyl alcohol, 29% water and 1% glycerol. The gel had a density of 0.886 g/ml at 25°C and viscosity of 70,000 cps at 25°C. The samples were measured

using an analytical balance to get the proper ratio of copper and nickel powders with the binding agent.

To consistently mix the paste, an electric centrifugal mixer (Flacktek (Model DAC 150.1 FVZ-K) was used. Paste formulations were mixed for times varying from 30 to 60 seconds and speeds from 1500 to 3000 rpms. 8–12grams of paste were mixed at a time in PP 50 mixing cups. The mixer properly distributed the powders evenly while eliminating air bubbles and left behind a homogenous paste.

2.   Rheometry

The paste mixture was produced and sent to the National University of Columbia to measure the shear characteristics of the paste formulation. The equipment used to measure the shear stress, shear rates, and viscosity was a Bohlin C-VOR Shear Rheometer. The parameters of the Rheometer were as follows:

<div align="center">

Analysis type: Controlled rate
Min share rate (1/s): 0.1
Max share rate (1/s): 1000
Delay time: 5 s
Integration time: 60 s
Temperature: 25 C

</div>

Table 1.   Samples Tested in Rheometer

Sample	Composition
1	Pure gel
2	1 g. gel + 0.611 g. Ni(5μ)
3	1 g. gel + 0.611 g. Ni(nano)
4	1 g. gel+ .50 g Ni(nano) + 0.50 g Cu(micro)

B.   3D PRINTING

Two different printers were used in the experiment. The first was an Ultimaker 2+ 3D, which supports a variety of different materials. The second printer used was a SE3D bio-printer, acquired with funds provided by NPS Naval Research Program (NRP).
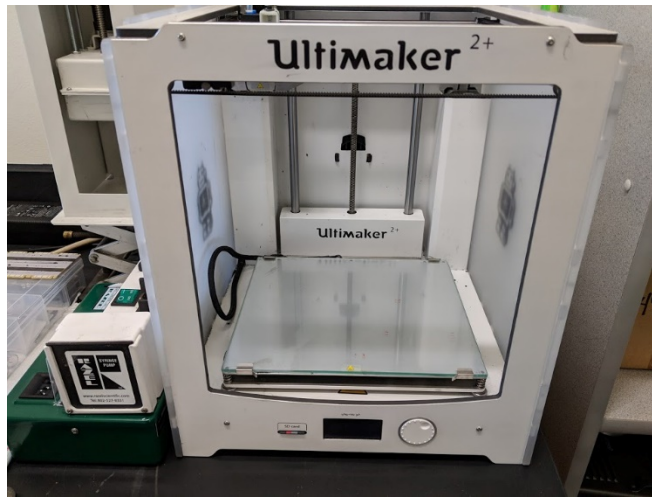
Figure 2.   Ultimaker 2+ Printer

The 3D extrusion printers place the material layer by layer in pre-determined patterns created by the user from a stereolithography (STL) computer aided design (CAD) file. The STL files used were created using CAD software. The initial files used are tensile specimens with dimensions in accordance with ASTM E8 [11]. The tensile shape is shown in Figure 3, which allowed for simpler characterization and testing.
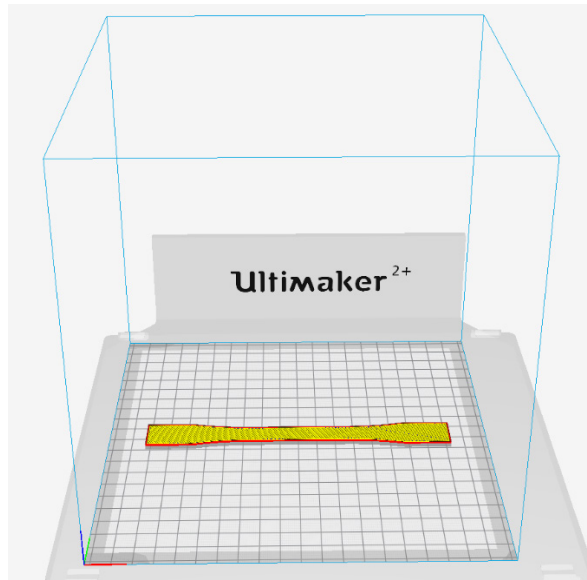
Figure 3.   Ultimaker2+ Software

The paste settings used were found through trial and error to find the optimum printing settings, which allowed for consistent and acceptable specimens for analysis. Printer speed, size, layer height, Infill density, pattern, and print cooling were changed based on how the paste was extruded and what the finished samples looked like.

Table 2.   Ultimaker 2+ Setting

Setting			
Material	Custom	Print speed	60 mm/s
Profile	Normal 0.15mm	Print cooling	enabled
Bottom layers	6	Fan speed	100%
Infill density	20%	Plate adhesion	Brim
Nozzle	0.8mm	Layer height	0.15mm
Wall thickness	0.9mm		

The plastic nozzle attached to the printer was a 0.84mm inner diameter polypropylene tip. The nozzle diameter changed the extrusion rate of the paste so different nozzles were tested to find the optimum extrusion rate based on printing speed, syringe extrusion speed, and nozzle diameter.

1.   Syringe Pump

An aftermarket syringe pump (Razel Model R99-FM) shown in Figure 4 was used to better control the speed at which the paste is extruded into the 3D printer. The syringe was filled with the metal paste and placed into the syringe pump for printing. 3/8-inch plastic tubing was used to deliver the paste from the syringe to the printer and the printer nozzle tip through a plastic adapter.

Figure 4.   Syringe Pump (Razel R99-FM Syringe Pump)

2.   Printing

Once the printing apparatus was set up, the g-code file was transferred to the Ultimaker 2+ printer and loaded for printing. The process was then controlled through the printer interface. Three layers were used in the tensile specimen design in accordance with ASTM E8 for the sample shown in Figure 5 [11].

Figure 5.   Ultimaker Printing

3.   SE3D Printer

The SE3D printer shown in Figure 6 supported printing liquids, hydrogels, and polymers with the use of 5mL and 10mL syringes. The SE3D printer was able to extrude the paste formulations at a lower concentration of binding agent. The minimum percentage of binding agent used in the SE3D printer was 42% gel and 58% metal powder by weight.

The printer also used a direct drive extrusion system that enabled the paste to be directly extruded from the syringe and therefore required less paste and no feed hose. A reduction in paste also limited the separation caused by settling. A separate extrusion pump was used which resulted in lower shear rates of the paste. The extrusion issues from the Ultimaker 2+ printer were resolved with the new 3D printer designed for bio printing materials. The printer also had a retraction capability that allowed liquids to be retracted between prints and during pauses, which preserved the shape of the samples.
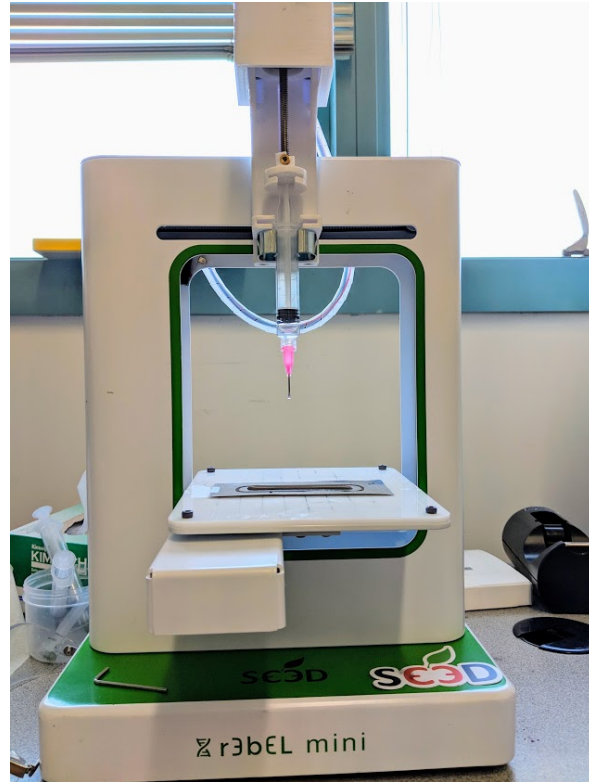
Figure 6.   SE3D R3bEL Mini Printer

4.   Drying

Once the file is finished printing, the material is allowed to dry in humidity controlled cabinets before handing. The post-printed products are soft and fragile because the powders have not been exposed to the correct conditions to fuse together and therefore must be handled with care. The samples are left in the cabinet for 24 hours to completely dry before they can be transferred for post-processing.

5.   Heat Treatment

The post-treatment process for the metal paste samples consisted of sintering at high temperatures for extended periods of time in an inert gas. The sintering process allowed the copper and nickel particles to bond together and recrystallize into a solid material. Sintering also burned off the binding agent, leaving behind only alloy material.

The phase diagram for copper and nickel is shown in Figure 7 and was referenced to determine the sintering temperatures for a desired phase of CuNi. In the case of copper

and nickel, they are isomorphous and therefore are completely soluble in each other. Both have face-centered cubic crystal structures, which enables the particles to be closely packed and fuse together to form a solid alloy.
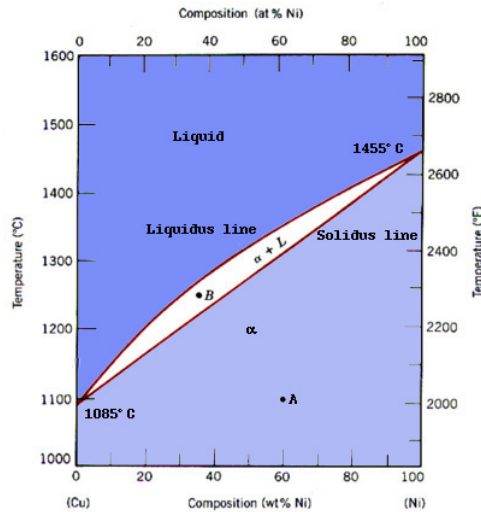
Figure 7.　Copper-Nickel Phase Diagram. Source: [12].

a.　Furnace

In order to sinter the metal powders together, a tube furnace was used to reach the sintering temperature. The furnace used an airtight glass tube, which was purged and filled with Argon gas to prevent reactions and oxidation from occurring with the samples. The samples were placed in crucibles and then centered in the glass tube. The specimens were then gradually heated to 1000°C and left to sinter for four hours before cooling back down to room temperature.

b.　Hot Isostatic Pressing

Hot isostatic pressing (HIP) is a method of heating a material while applying isostatic pressure in an inert gas to prevent any oxidation or chemical reactions. HIP was used to sinter the material while reducing the porosity and increasing the workability of the alloy. The HIP model used was an AIP 6–45H rated to 30,000 psi (207 MPa) with the following settings listed in Table 3.

15

Table 3.   HIP Conditions

Batch	Temp.	Pressure	Time, rate	Cooling, rate
Group 1	1000°C	138 Mpa	5 hours, 10°C/min ramps	Cooled for 90 minutes, 10°C/min ramps
Group 2	1000°C	172 Mpa	5 hours, 10°C/min ramps	Cooled for 90 minutes, 10°C/min ramps
Group 3	1000°C	172 Mpa	5 hours, 10°C/min ramps	Cooled for 90 minutes, 10°C/min ramps
Group 4	1000°C	207 Mpa	12 hours, 10°C/min ramps	Cooled for 90 minutes, 10°C/min ramps
Group 5	1000°C	241 Mpa	12 hours, 10°C/min ramps	Cooled for 90 minutes, 10°C/min ramps

C.   MATERIAL CHARACTERIZATION

After the post-processing of the samples, the samples were examined with various equipment to determine the phases, composition, and metallography of the sintered alloy.

1.   Sample Preparation

Samples were prepared for characterization with SEM, EDS, and hardness measurements by placing a small piece of the material into a Condufast puck using a mounting press machine. The conductive puck prevented the samples from having a charge when the electron beam is applied.

Figure 8.   HIP Cu(micron)-Ni(micron) at 172 Mpa/1000°C

The samples were then sanded using an Ecomet 4 variable speed-polishing machine. The following settings were used in the automatic sander:

Table 4.   Ecomet 4 Polishing Settings

Setting	Measurements
Pressure	22.24 N
Speed	150 rpm
Sandpaper	500, 800, 1200, 1500, 2400
Polishing Compound	Alumina (1 µm and 0.05 µm)

The polishing time for each grit was 30 minutes until the final polish, which used a micro-cloth and Alumina suspensions in water for 60 minutes. The polished samples were then cleaned with ethanol and dried before starting the material characterization.

2.   Optical Microscope

The optical microscope used was a Epiphot 200 inverted metallurgical microscope which was able to take images up to 100x magnification and both Brightfield and Darkfield

17

images. The microscope allowed for pictures of at the microscopic level to be taken and used in ImageJ software for determining volume fraction of the porosity in the sample through point count analysis. Samples prepared and polished after post-treatment were viewed in the optical microscope to observe the metallography of the sample and the grain characteristics.

a.   ImageJ

ImageJ uses pixel value statistics to determine the area and size of different colors in a picture. The program takes a picture and converts it into binary colors which is then used to count the number of light versus dark pixels. In this case, the dark pixels represented porosity in the specimen shown in Figure 9. Micrographs were saved from the optical microscope of different locations in the sample and uploaded into ImageJ for a quantitative analysis of the porosity [13]. Volume fraction of the sampled is determined through a point count analysis. An average of the volume fraction in ten different locations were taken for each sample with the standard deviation. The porosity size distribution (PSD) was taken and graphed to compare the porosity in each sample.
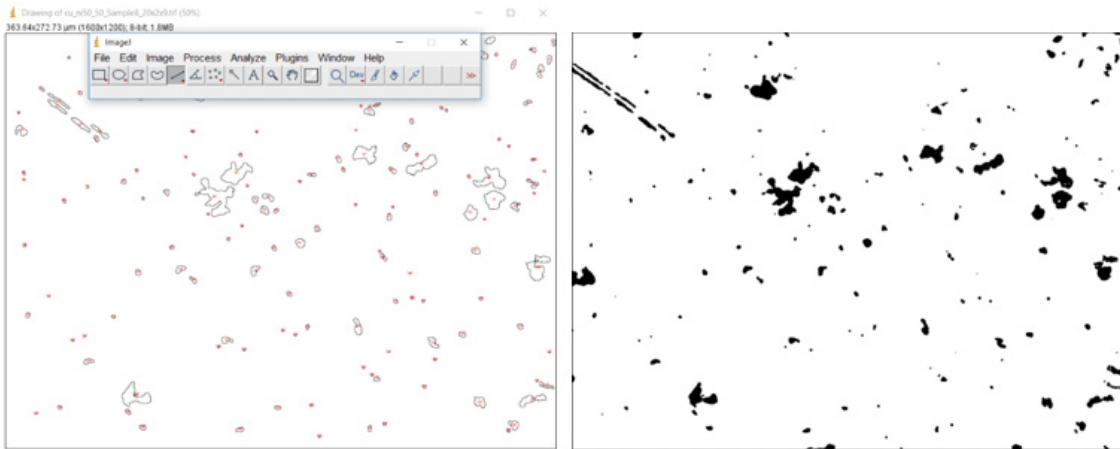

Figure 9.   ImageJ Program with CuNi Sample at 20X Magnification

3. Scanning Electron Microscope

The microstructure of the alloy was observed using a Zeiss Neon 40 Field Emission Electron Microscope (FE-SEM). The SEM emitted high velocity electrons that would impact the surface of the sample and force Secondary Electrons (SE) to scatter. The scattered electrons are then detected and are displayed in an image based on the topography of the surface. SEM settings were set as Electric High-Tension Voltage (EHT): 20.00 kV, WD: 5mm, Image settings BSE2, BSD.

The SEM was equipped with a Back-Scattered Electron Detector (BSE) which was used to determine the existence of separate phases in the alloy. The BSE works using back-scattered electrons off the surface of a material based on sample composition. The BSE would confirm if a solid, single phase of CuNi alloy was created after the sintering process.

a. EDS

Energy-dispersive X-ray Spectroscopy (EDS) was incorporated with the SEM to determine the elemental composition of the alloy. The EDS emits a high-energy electron beam that forces electrons from the outer shells of the specimen. A spectrometer then counts the number and energy levels of the X-rays. Each element has characteristic X-rays, which are different due to their atomic structure. The number or count of X-rays allows the chemical composition to be found.

A 30mm aperture was used for the EDS to allow additional X-rays to be detected. At least 30,000 counts were recorded before saving the data. An EDS analysis was also conducted to determine if oxidation or other reactions occurred within the sample.

4. X-ray Diffraction

Post-treatment specimens were characterized using x-ray crystallography to determine their crystalline structures. X-ray Diffraction (XRD) works by diffracting incident x-ray beams off of a sampled. The unique angles and intensity of the diffracted beams are measured and are matched with specific elements. A Rigaku Miniflex 600 X-ray Diffractometer was used in the study.

The XRD works using Bragg's Law shown below which explains how radiated incident x-ray beams are diffracted off a crystalline surface. The crystals are oriented in lattice planes in which their orientation is defined by its Miller indices. The distance between planes is known as the d-spacing and can be found using the XRD. The characteristic x-rays are diffracted at an angle, Θ (theta).

$$\lambda = \mathbf{2}*d*sin\theta$$

The XRD was used with the CuNi specimens to determine the presence of oxidation or other heat treatment byproducts from the binding agent. The XRD used a nickel filter so the incident x-ray was a single wavelength and removed excess noise. Samples were prepared by grinding the specimen in a mortar and pestle into a powder and pressed into a monocrystalline Silicon sample holder. A single-crystal holder ensured no background noise was observed from 20 to 120 degrees of Cu Ka X-rays.

5.   Simultaneous Thermal Analysis (STA) TGA/DSC

Thermal analysis of the metal powder and sintered specimen were conducted using the 449 F3 Jupiter STA machine. The STA was a single machine that used both thermogravimetric analysis (TGA) and Differential Scanning Calorimetry (DSC). The DSC recorded the heat flow with respect to time and temperature while the TGA recorded the weight change versus time and temperature. The STA measured the change in weight of a specimen, which was used to determine when the binding agent was burned off and the sintering temperature.

The samples were prepared by grinding it into a powder with a mortar and pestle. The powder was then placed into an alumina crucible before placing in the STA. An empty crucible was also placed into the STA as a reference for the sample. The STA heated the specimen to 1030°C at a rate of 20°C/min. in Argon gas. The inert gas prevented oxidation of the sample, which would affect the weight and sintering temperature. The data was then recorded for analysis by graphing the weight versus time and temperature as well as the heat flow versus time and temperature. From these analyses, the sintering temperature of the sample was able to be determined.

6. Hardness Testing

The specimen's hardness was measured using DuraScan 50 5GMicro-hardness tester.. The machine used the Vickers method to determine the hardness by taking the force applied and dividing it by the surface area of the indentation crated on the specimen. A load of HV0.05 kgf was used to test the CuNi alloy samples. Ten separate test points were used for each sample to get an average value of the hardness. The hardness data was then compared to the HIP conditions and porosity for each respective sample.

THIS PAGE INTENTIONALLY LEFT BLANK

III. RESULTS

A. PASTE FORMULATION

The first binder agent employed, a hydrocarbon saturated paraffin, was mixed with the metal powder and heat treated to determine its decomposition temperatures. According to STA data, the binder was effectively removed in oxygen containing atmospheres at temperatures that will not oxidize the Ni or Cu powders. However, the viscosity of the paraffin-metal powder mixtures was too high to be effectively used in the extrusion printers. An alcohol-based gel, consisting of ethyl alcohol, glycerin, propylene glycol and water, as described in the last chapter, was selected as a binding agent.

The metal powders employed were analyzed by SEM to determine their shape and size distributions. Figure 10 shows at even distribution of nickel nanopowder, which was mixed with copper nanoparticles to form the first mixture, employed.
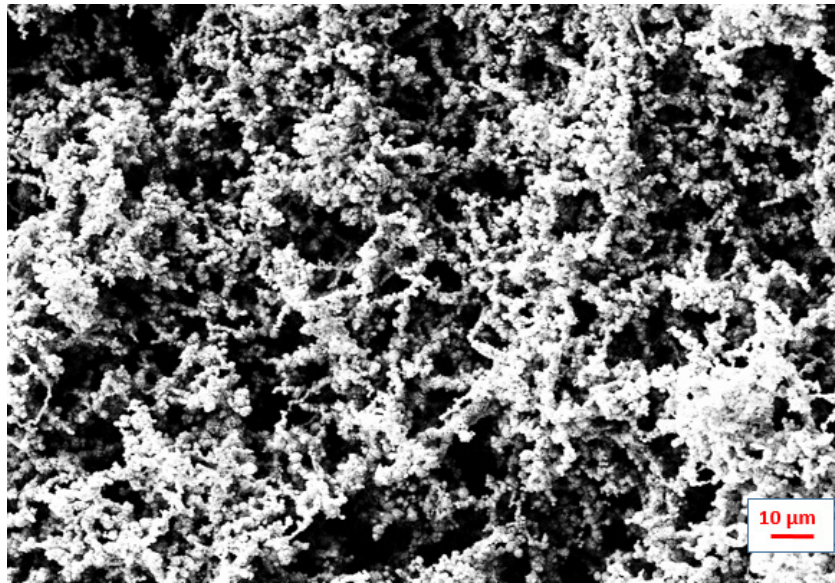

Figure 10.   SEM Image of Pure Nickel Micron Powder at 500x Magnification

When nanoparticulates were used as raw materials, the feed hose showed a separation between the powder and the gel when the syringe is near half-extruded, as seen

in Figure 11. The separation in the tubing resulted in only gel being extruded during parts of the printing and causing the samples to be unusable. The separation was attributed to an increased shear rate by the syringe pump and a small feel hose. The rheological properties of the gel and powder mixture were analyzed to confirm the cause of separation and clogging of the printer extruding system.

Figure 11.   Ultimaker 2+ Printer Feed Hose

1.   Rheometry Data

The viscosity of the pastes at different shear stresses was measured in gel-metal mixtures containing either nano-size or micron-size powders to help understand how the powder reacts with the binding agent when stress is applied.

For pure gel, the analysis showed that the viscosity linearly decreases as the shear rate increases, that is, the gel sample tends to flow better as the load increases, the viscosity changes 3 orders of magnitude as the shear rates is incremented from 0.1 to 1000 1/s. The shear rate and shear stress have a liner relationship, as indicated for Figure 12. When micron size particulates of nickel are added to gel, the behavior observed in the gel remains, linear decrease in viscosity is observed as shear rate is increased, as shown in Figure 13. The addition of nanoparticle of Ni to the gel show a completely different interaction, the

viscosity decreases linearly until the shear rate reaches 100 1/s, where the slope of the curve dramatically changes slope, indicating less resistance to flow (see Figure 14). The viscosity observed from the Ni nanopowder and binding agent indicate that the mixture acts as a thinning agent when the particulates are in the nanometric range, providing an explanation to why the paste segregates in the hose and extruding systems of the printer. Given the linear change in viscosity observed in the micron Ni mixtures, these were used to perform any subsequent printing experiments.
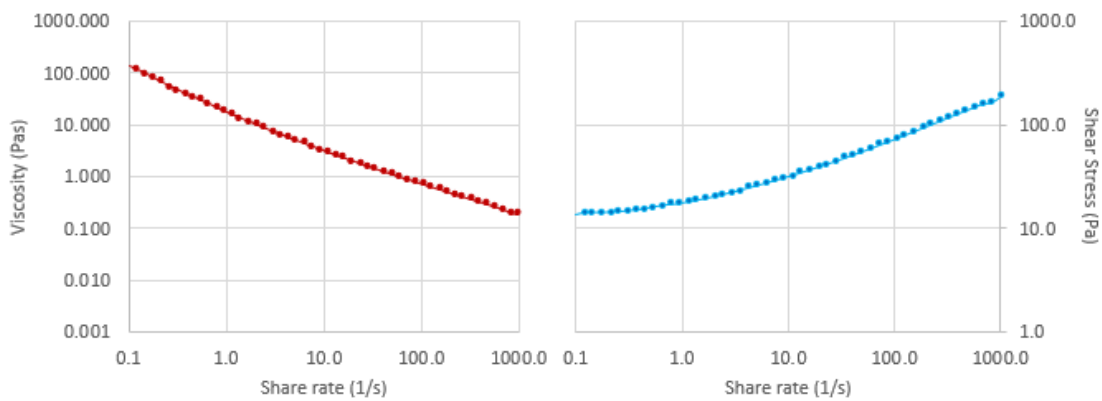
Figure 12. Viscosity versus Shear Rate(left) Shear Stress versus Shear Rate (right) of Pure Gel at 25°C
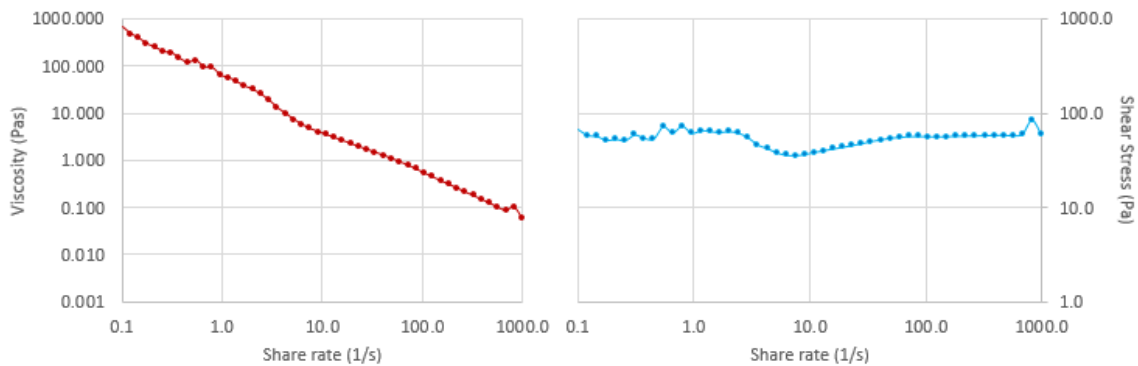
Figure 13. Viscosity versus Shear Rate(left) Shear Stress versus Shear Rate (right) of Ni Micron and Gel at 25°C

The shear stress increased proportionally with the shear rate for the pure gel while the nano-nickel decreased with shear rate and the micro-nickel remained relatively constant. The same tests were conducted with copper and nickel nanopowder mixed together with the results shown in Figure 15. The nanopowder mixture reacted in a similar manner as the nano-nickel with the shear rate dropping at 100 1/s shear rate from a shear stress of 100 Pa to 5 Pa.
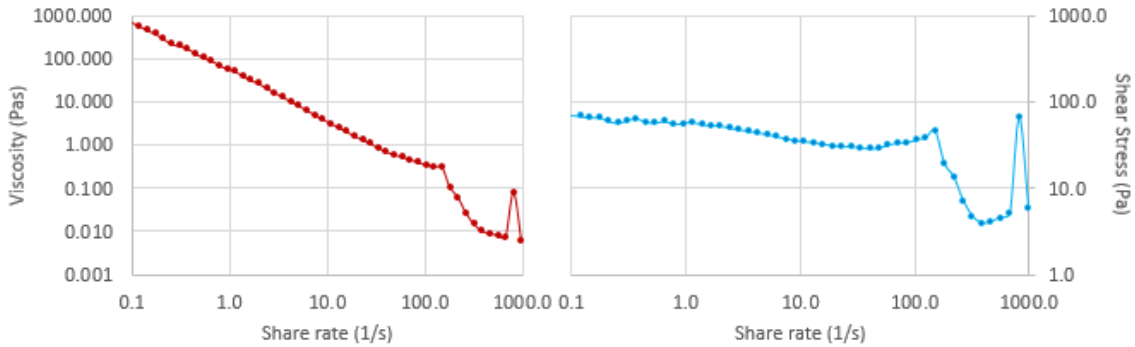

Figure 14.   Viscosity versus Shear Rate(left) Shear Stress versus Shear Rate (right) of Ni nano and Gel at 25°C
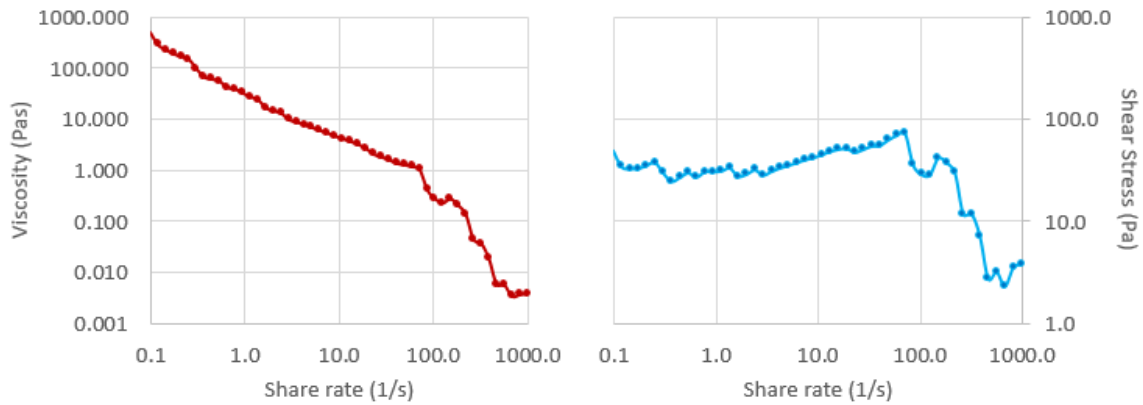

Figure 15.   Viscosity versus Shear Rate(left) Shear Stress versus Shear Rate (right) of CuNi nano and Gel at 25°C
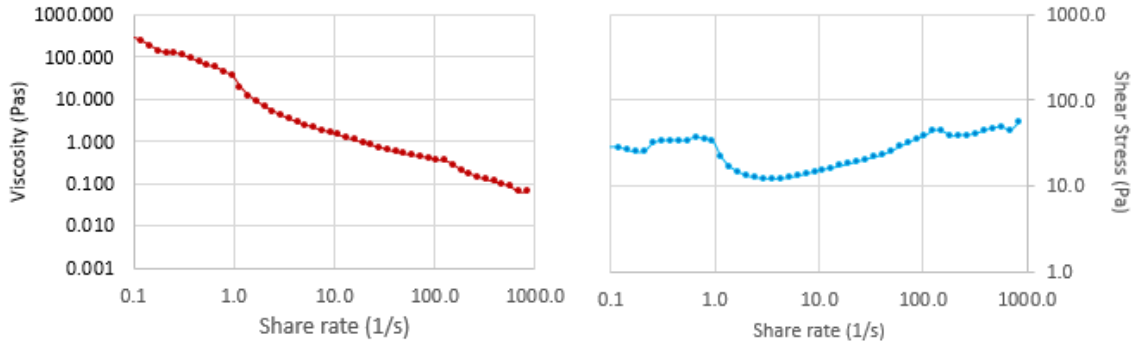
Figure 16.   Viscosity versus Shear Rate(left) Shear Stress versus Shear
Rate (right) of CuNi micron and Gel at 25°C

The paste formulation acts as a non-Newtonian fluid when shear force is applied. This justifies why the nozzle was being congested when the extrusion speed was high for the metal powder mixed with the binding agent. In order to print with the desired binding agent, the extrusion rate and printing speed were decreased so that the shear rate was lowered and the viscosity was high enough to print consistently with. The SE3D printer allowed for extrusion rate control and printing speed adjustments while printing and allowed for better control of how a sample was printed.

The thinning properties of the nanopowder can be advantageous when used in other applications. Lotions, paint, and thin coatings are a few examples where the low viscosity as a result of the nanopowder interaction with a binder can be used. Gaharwar et al. has found applications in the medical field for shear-thinning nanocomposites to prevent blood clots [14]. For 3D applications, it was determined that a shear rate below 100 1/s was required to be able to extrude nanopowder material to prevent the thinning of the paste in a paste formulation.

2.   3-Printing

After a suitable binding agent was chosen, the metal micron powders and binding agent were mixed together using the dual asymmetric mixer. The ratio of binding agent to metal powder was adjusted to a) reduce the amount of gel required, thus the sample will suffer less shrinkage and porosity, increasing the possibility of the particulates to be in

close contact increasing the strength of the material and b) enough gel to have a paste that could be easily extruded. Using the SE3D printer, a 46% powder by weight and 54% binding agent was the optimal ratio the printer could successfully print and still hold its shape.

The mixture was then placed in a plastic 10ml syringe and printed using the desired g-code. Multiple layers of the design were printed by using the cooling fan attached to the printer to dry the previous layer shown in Figure 17. As result, we were able to produce solid shapes in a 'green' state, that is, compacted powders with the desired shape but no mechanical robustness. The "green" samples are typical in other powder metallurgy 3D printing techniques such as binder jetting. The sample in the "green" state shown in Figure 18 requires heat treatment in order for the powder particles to fuse together and form an alloy.
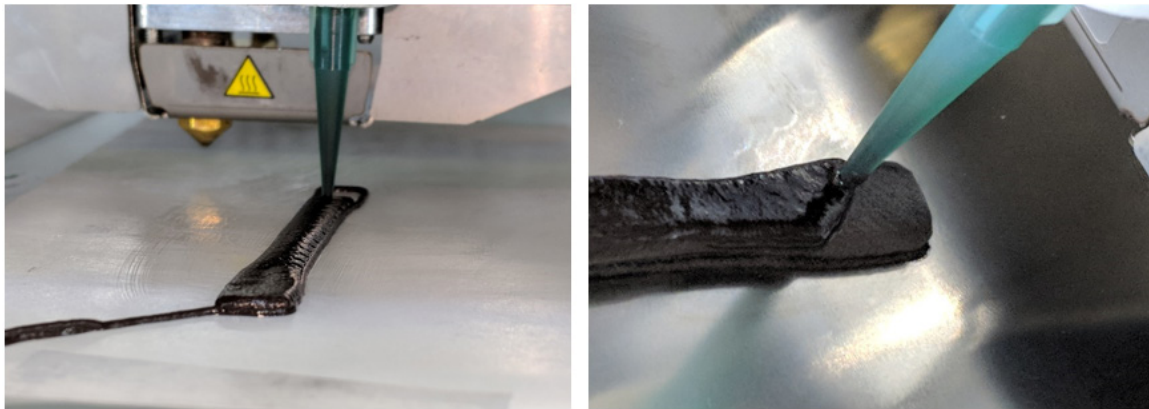

Figure 17.   Ultimaker 2+ Printed CuNi samples
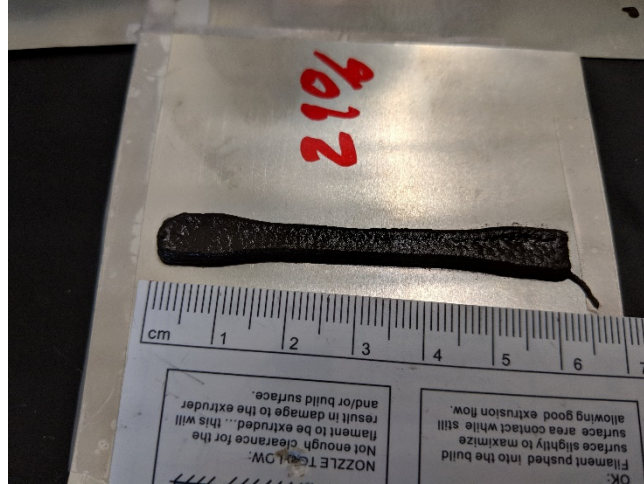
Figure 18.   Air-Dry Sample

Samples removed from the printer were left to air dry in a desiccator overnight before further handling. Drying times varied from 12–24 hours before the sample could be removed from base plating and handled for post-treatment processes if the drying process was conducted at room temperature. Higher temperature will result is shorter drying times; however, will also cause rapid shrinkage that could fracture the specimen. The samples held their shape and could be lightly handed but was too fragile for strength testing. The specimens were sent to off for heat treatment in order to fuse the metal powders together and form an alloy.

Figure 19.   3D Printing Process by Active Print (left), Post-Print(middle), and Post-Sintering(right)

B.   POST TREATMENT

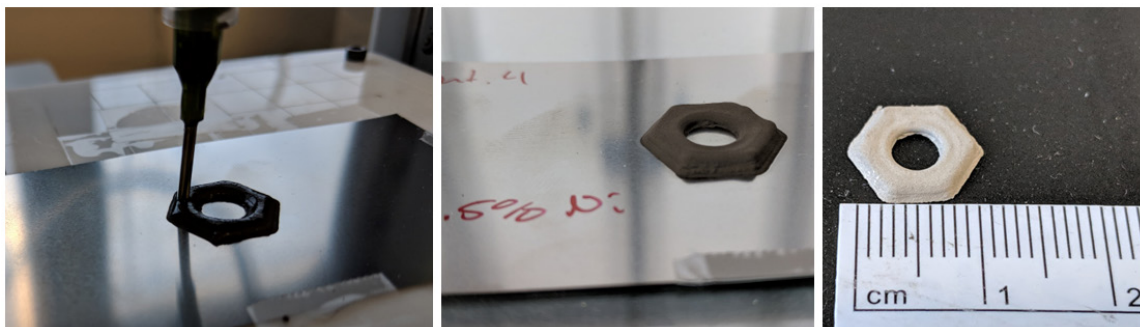The "green" products from the printers were sent to American Isostatic Presses (AIP) to conduct the HIP treatments. The samples were placed in an airtight chamber and purged with Argon gas. The temperature and pressure in the vessel were steadily increased up to 1000°C and 138 Mpa, as shown in Figure 20. The temperature increased at a constant rate of 10°C/sec, remained at 1000°C for 10 hours and then cooled at the same constant rate for sample set 2. The first set kept a constant temperature rate for heating and cooling; however, it is noted the pressure decreased during the sustained temperature phase.
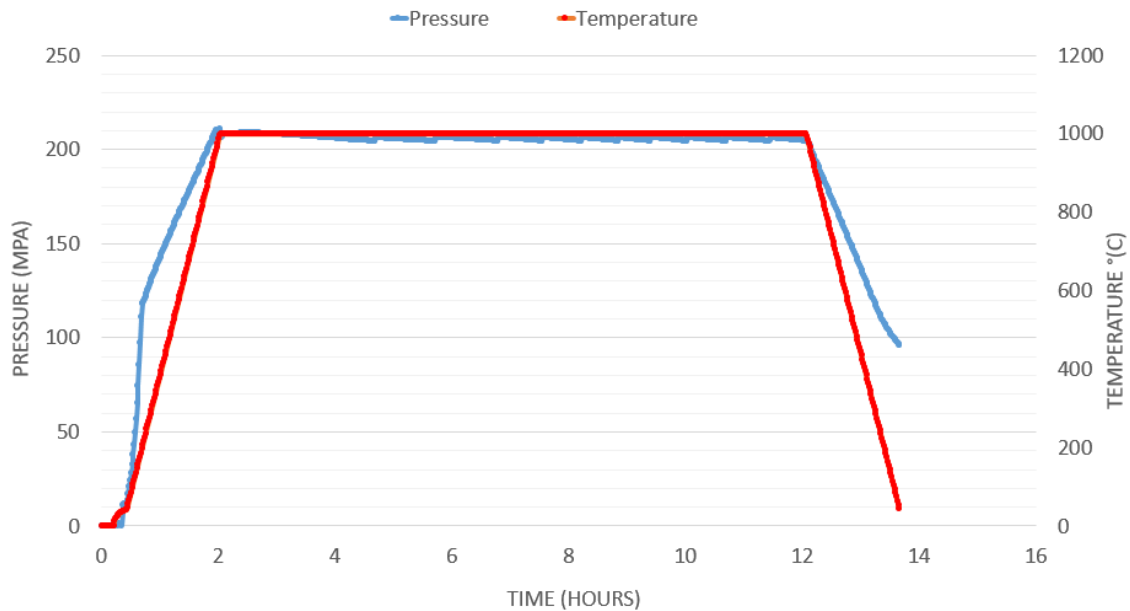
Figure 20.   HIP Temperature and Pressure Profiles for Sample Set 1

The steady low cooling rate allowed the grains to grow larger with a coarse grain structure and in turn affected the material properties. Slower cooling rates resulted in lower hardness but higher ductility in the samples. The high pressure was used to reduce the porosity, and improve the mechanical properties of the material. Tightly packed particles allowed stronger bonds to form between the metal powders while any voids or cavities inside the alloy would decrease the strength and hardness of the materials.

30

Argon, an inert gas, was used to prevent oxidation of the metal during the HIP process. The heating chamber was purged of atmospheric gases to prevent reactions with the specimen.

Figure 21.   HIP Temperature and Pressure Profiles for Sample Set 2

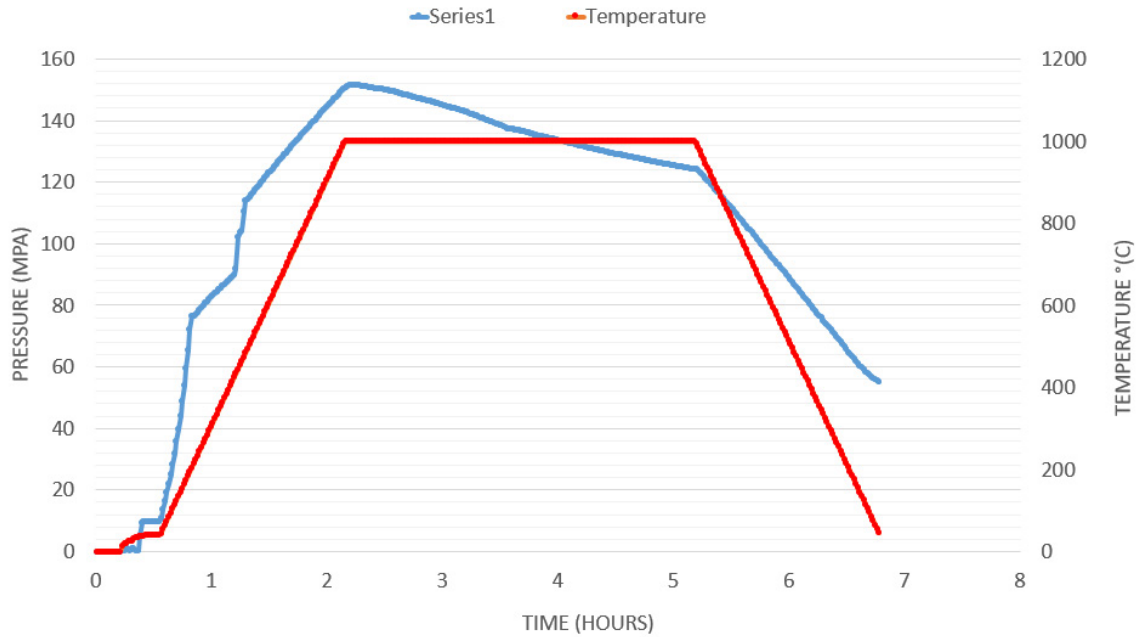Samples returned from HIP decreased evenly in size in the X, Y, and Z directions. The decrease in size was expected due to the high pressure forcing the particles closer together and removing vacant spaces. The high temperature also burned off the binding agent, which accounted for 48% of the weight of the specimen in Figure 22 The average size decrease was 35% in each direction. The weight of the micron powder mixture decreased by 36%. Figure 22 shows the shrinkage of a sample of Cu-Ni micron HIP at 207 Mpa and 1000°C. The specimen in the center of Figure 22 corresponds to the part after being HIP at 207 Mpa in 1000°C. The red marker indicates the size of the green body before heat treatment. Kumar et al. found that copper micro-powder samples created through binder jetting under heat treatment in a box furnace at 1075°C for three hours resulted in shrinkages of 14.14% to 18.57% [6]. HIP treatment after the initial sintering at 1075°C and 207 Mpa (206.85 MPa) resulted in further shrinkage of 15.52% to 19.70% [6].

Binder jetting 3D printing of copper paste by Sanchez et al. [5] also experiences uniform shrinkage as much at 77%.
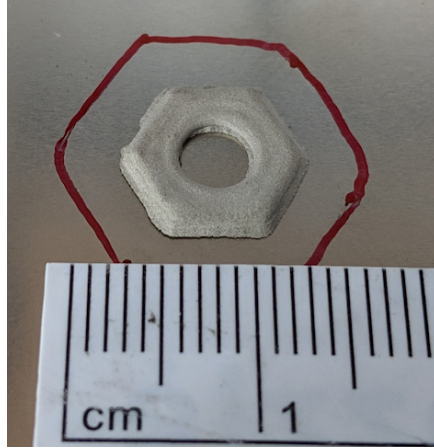
Figure 22.   Cu(micron)-Ni(micron) after being 3D printed and HIP at 207 Mpa in 1000°C

C.   OPTICAL MICROSCOPE

The optical microscope was used for determining the metallography of the samples through which the grain structure, size, shape and patterns of the sintered alloys were studied. The OM also allowed for estimations of the porosity in each specimen using ImageJ software. Micrographs of the specimens were taken at 2.5, 10, 20, 50 and 100x magnification to observe the effects on the microstructure of each sample after heat treatment.
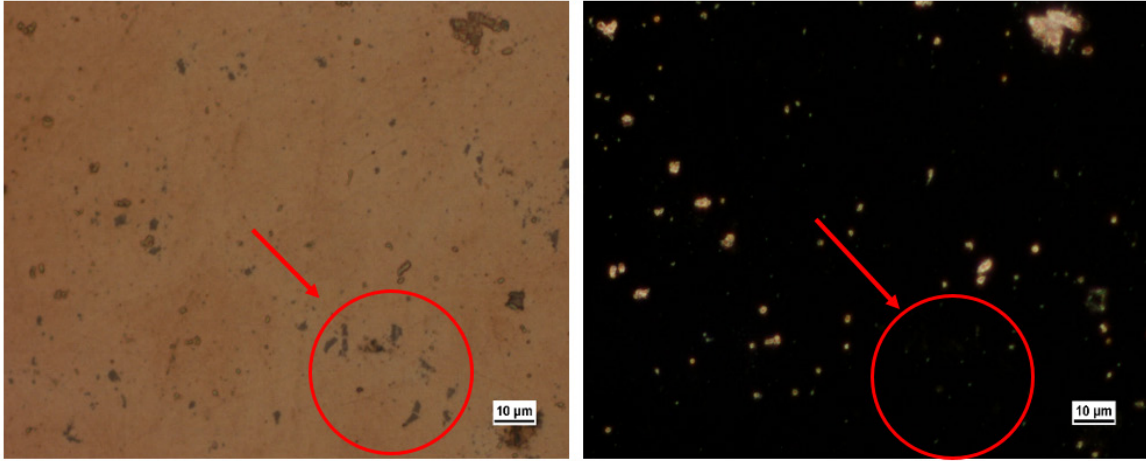
Figure 23.   Lightfield Image (left) Darkfield image (right) of CuNi HIP
Sample 2 at 50X Using OM

The darker spots in Figure 23 on the left are areas where light is not as reflective and represents possible pits or pores in the sample. Using the Darkfield feature of the microscope with the image on the right, the unscattered light from the lens is not reflected and therefore shows the surface being dark. The red circles in Figure 23 show where dark spots are not shown in the Darkfield image. These spots are a different phase of material and not voids in the sample. The lighter areas highlight porous areas in the sample but do not show depth. The porosity between the different post-treatment pressures can be observed in Figure 24. The size and number of the voids decreased as a result of the increased sintering pressure.

Figure 24.   HIP 138 Mpa (left), 172 Mpa (middle), 207 Mpa (right)
Samples Optical Micrographs

The size of the void shown in Figure 25 was approximately 7 μm in diameter. Further analysis on porosity size and distribution of the sample was conducted using ImageJ software.
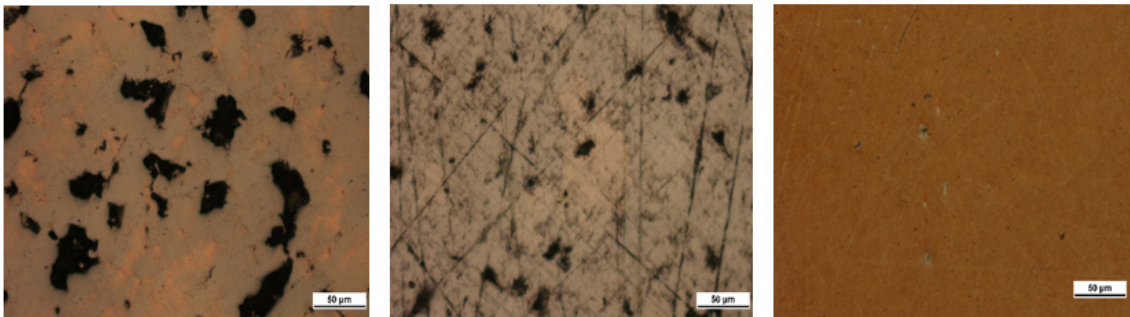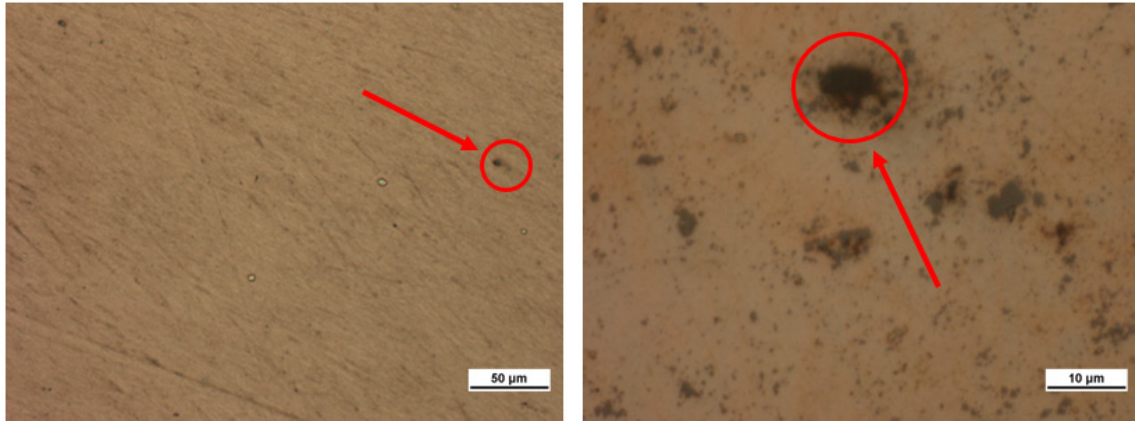

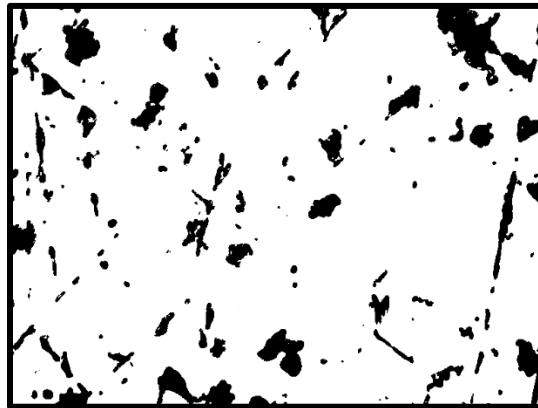Figure 25.   Voids in HIP Sample at 20x Magnification and 100x Magnification

Figure 26.   ImageJ software binary picture of CuNi sample at 50x magnification

Table 5.   Particle Size Calculations Images A, B, C of HIP 172 Mpa

	Image A	Image B	Image C
STDV	88.64	101.55	272.63
Vol. Fract.	84.30%	82.47%	82.75%

Sample A was 84.3% copper-nickel while Sample B was 82.47% and Sample C was 82.75%. That is, the void space was calculated to be between 15.7 and 17.5% of the total area. The larger difference of porosity in the samples are attributed to the random areas chosen in the sample and an uneven distribution of voids. Various locations contained difference sizes and uneven structures that were seen in the average grain sizes. The average standard deviation was 133.96 µm and the average occupied volume fraction was 78.13%. The error in the volume fraction can also be attributed to the noise cancellation of smaller grouped pixels radius 5 and under. Instances of the pixels that were removed included particles inside the darker porous spaces which adversely affected the volume fraction. Other difficulties experienced using ImageJ included higher porosity near the edges of the sample while images closer to the center had a higher density. Lastly, scratches on the sample from polishing left long cuts, shown in Figure 32, which the program counted as porosity.

Average values of the sample taken from different images was then used to give an estimate for the porosity of samples after post processing techniques. The average porosity of ten images for each samples are given in Table 6. The porosity decreased with higher pressures and longer sintering times. HIP conducted on copper micron powder via inject deposition has shown an increase in density from 92% to 99.7% of the theoretical density [6].

Table 6.   ImageJ Porosity Results

Pressure	Temp.	Time	Porosity
138 Mpa	1000°C	5 hours	17.53%
172 Mpa	1000°C	5 hours	17.02%
207 Mpa	1000°C	12 hours	10.56%

D. TGA/DSC

In order to compare sintering temperatures and times for the diverse powder formulations employed, simultaneous thermos-gravimetric and differential scanning calorimetry analysis were conducted. The copper and nickel nano-powders with gel showed a 3.54% decrease in mass at 1050°C, corresponding to the evaporation of volatile solvents in the gel. The DSC signal presented inflections in the curve for that transformation and for the sintering process/densification that the sample presented at 300°C temperature. Heat treatment in Argon gas prevented oxidation and other chemical reactions of the metals during sintering. The sample was heated to 1050°C for four hours then slowly cooled.

The DSC was used to determine phase transformation in during the heat treatment by comparing heat flux versus temperature and time. The initial dip in Figure 27 shows the sample going through an exothermic process of crystallization and therefore less heat is required to increase the temperature.
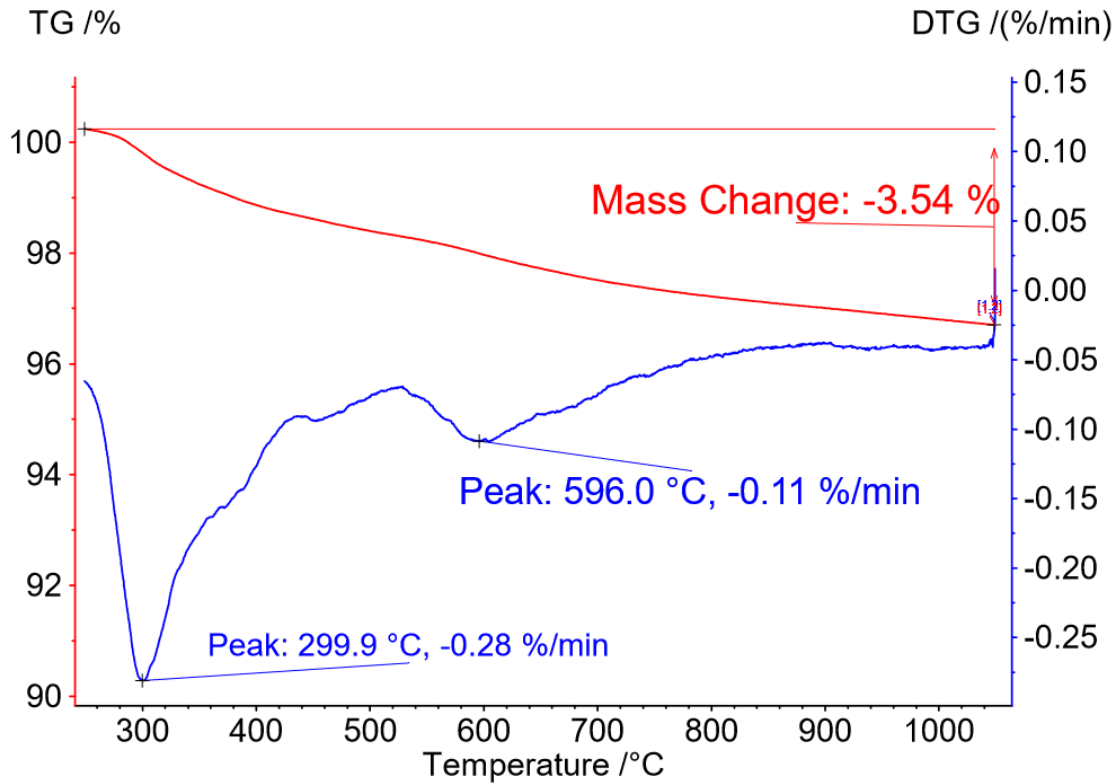
Figure 27. TG versus Temperature of Cu(nano) Ni(nano) in Argon
Gas

E.   SEM/BSD/EDS

The images in Figure 28 show the sintered CuNi alloy at the microscopic level. The coral like structure is the CuNi alloy while the dark voids are empty spaces that remained after the binding agent was burned off in the sintering process. The SEM showed the metal powder particles fused together, forming a single crystal phase. Figure 29 is an SEM image [15] of a similar CuNi alloy known as Monel 400, which contains a high nickel content. The coral-like microstructure of the Monel is similar to that of the samples post-heat treatment.
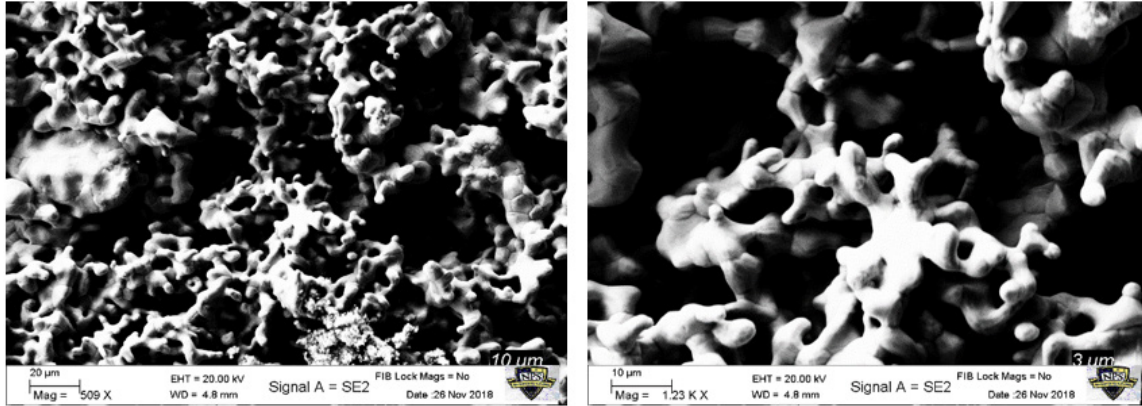
Figure 28.   SEM micrographs of Sample 2 Cu(nano)Ni(micro) 172
Mpa after HIP
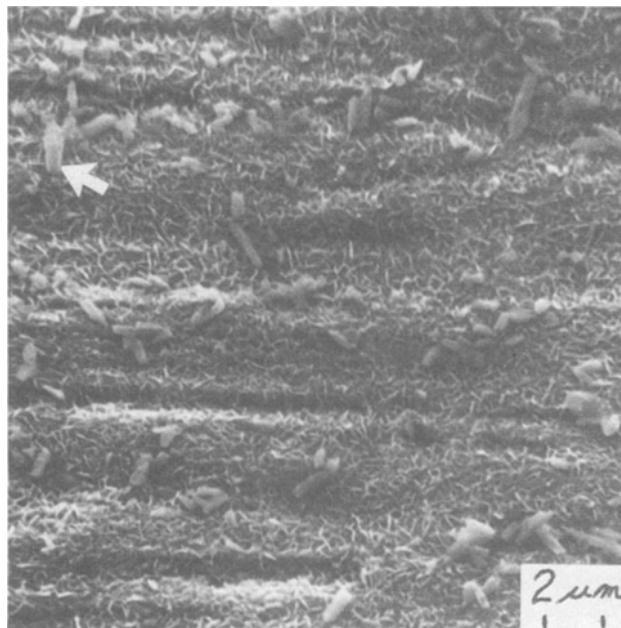
Figure 29.   SEM Image of Monel-400 [Source:15]

The high porosity in the first two samples were reduced with higher HIP pressure and longer sintering temperatures, as shown in Figure 30. The reduction in size and number of voids allowed for greater contact area between the metal particles, improving the material properties of the alloy. The resulting microstructure of the specimen was also examined for defects and contaminates from the binding agent and sintering process. Figure 30 was taken of a CuNi micro-powder after HIP which shows varying sizes of voids

present in the alloy. These empty spaces needed to be further reduced in order to increase the density of the alloy and its hardness. Herzog et al. found that porosity facilitates crack propagation, which decreases the material properties [16].
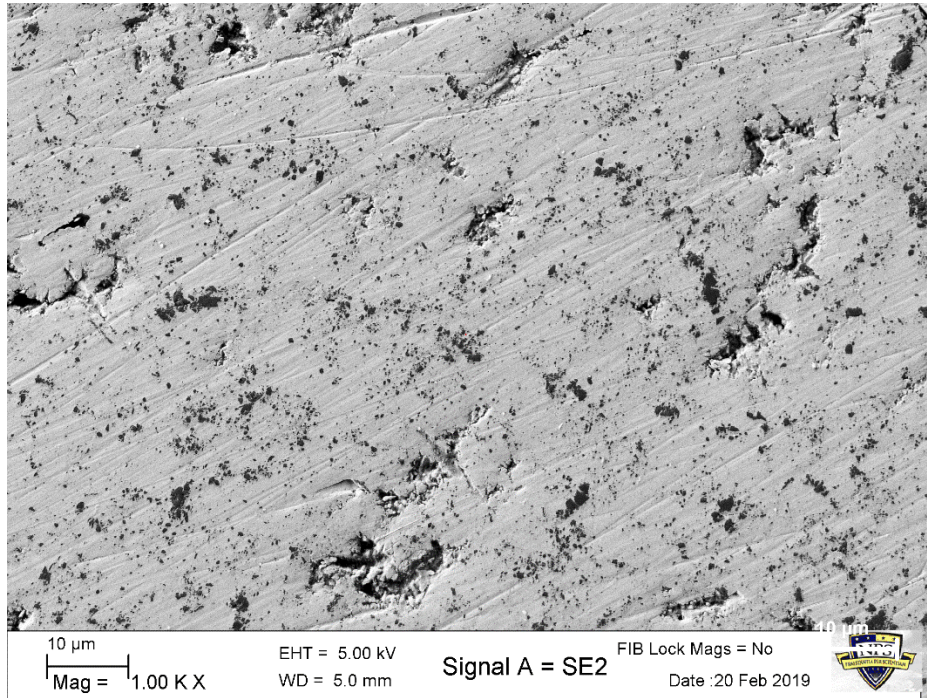
Figure 30.   SEM micrograph of Cu(micro) Ni(micro) at 207 Mpa
1000x magnification

The ratio of binding agent and CuNi powder also impacted the porosity in the sample. To lower the porosity, the minimum amount of binding agent to metal powder ratio that the 3D printer could successfully print was used. Figure 31 shows the larger and more frequent voids in the sample with a higher weight percent of gel in the sample. The sample on the right contained 2% by weight less binding agent and 2% more CuNi micro powder.
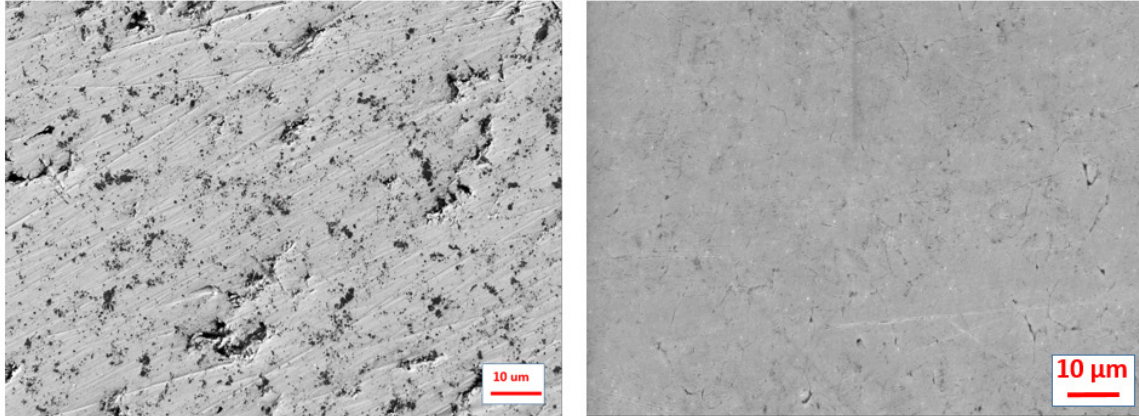
Figure 31.   Sample 9 (left) with 50% gel 50% micro CuNi powder,
Sample 8 (right) with 52% micro CuNi powder both HIP at 1000 °C for 12
hours

1.   Backscattered Electron Detection (BSD)

Backscattered electron detection (BSD) was used to determine phases with diverse atomic numbers in the sample. Figure 32 shows the before and after image of the BSE detector which validates that there is a single phase within the sample. An uneven mixture of copper and nickel can form cupronickel phases which contain higher nickel content.
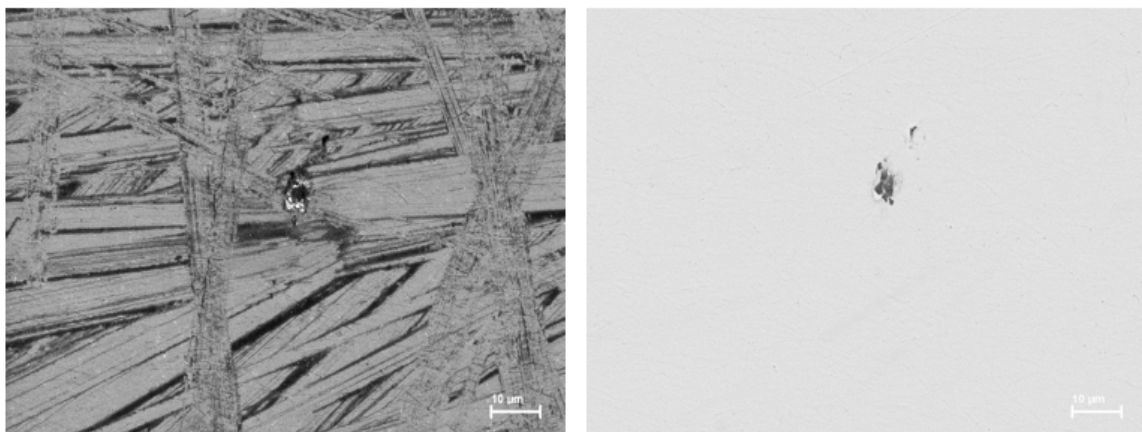
Figure 32.   SEM image (left) BSD image (right) 207 Mpa Sample 7 at
1000x magnification

2.   Energy Dispersive X-ray Spectroscopy (EDS)

Energy Dispersive X-ray Spectroscopy (EDS) was performed on the samples to determine the elements present in the metal alloy. EDS was useful in also determining if oxidation or other byproducts were left behind from the binding agent in the sample. The chemical composition of the sample is shown in Figure 33 and Table 7. The dark spot in the center of Figure 34 was found to be aluminum using EDS. The alumina particle was a result of the polishing process in which Alumina (aluminum oxide) of 0.05 micron was used to prepare the sample for the SEM and OM.
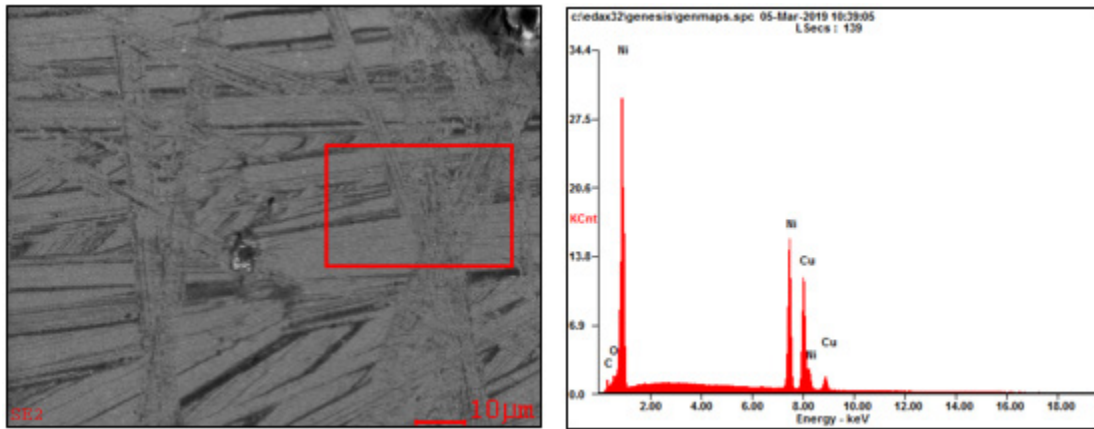
Figure 33.   EDS Image of 207 Mpa HIP Cu(micro) Ni(micro) Sample (left) and EDS Spectrum(right)

Table 7.   EDS Microanalysis of elements

Element	Wt%	At%
CK	04.46	18.57
OK	01.34	04.19
NiK	48.15	41.01
CuK	46.05	36.24
Matrix	Correction	ZAF

Element	Wt%	At%
CK	04.87	08.98
OK	33.04	45.77
AlK	49.64	40.78
NiK	04.46	01.68
CuK	07.99	02.79
Matrix	Correction	ZAF
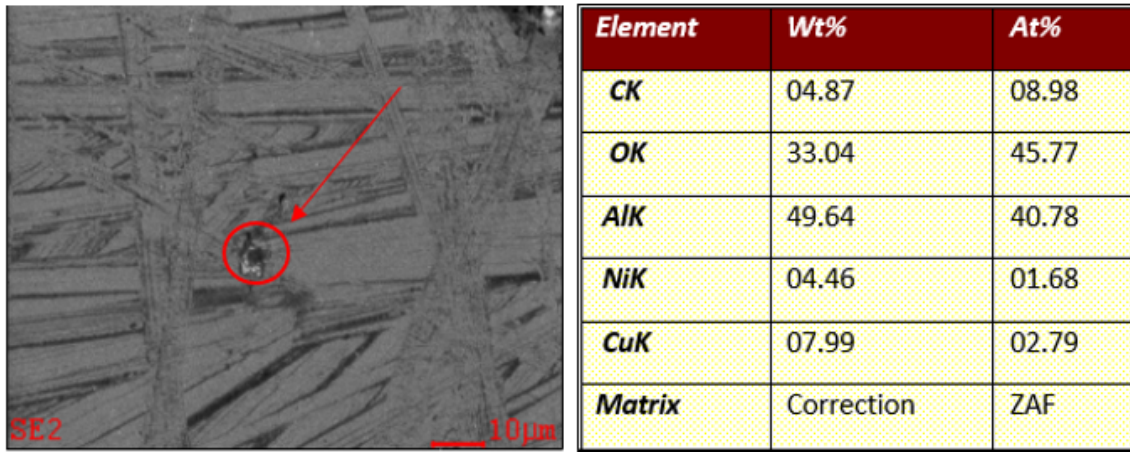
Figure 34.   EDS on Discoloration

F.   XRD

The sintered CuNi alloy was placed in an X-ray Diffraction machine to determine if the gel was completely evaporated and if byproducts were created during the sintering process. The sample contained 48% gel and 52% Cu(nano) and Ni(nano) powder which was HIP tested at 1000 °C for 3 hours. The 2-theta angle peaks match that of copper and nickel with no other chemicals detected as shown in Figure 35, thus, providing a proof of concept that neither the gel nor the post processing steps produce oxidation in the alloy and that the composition remains as targeted.
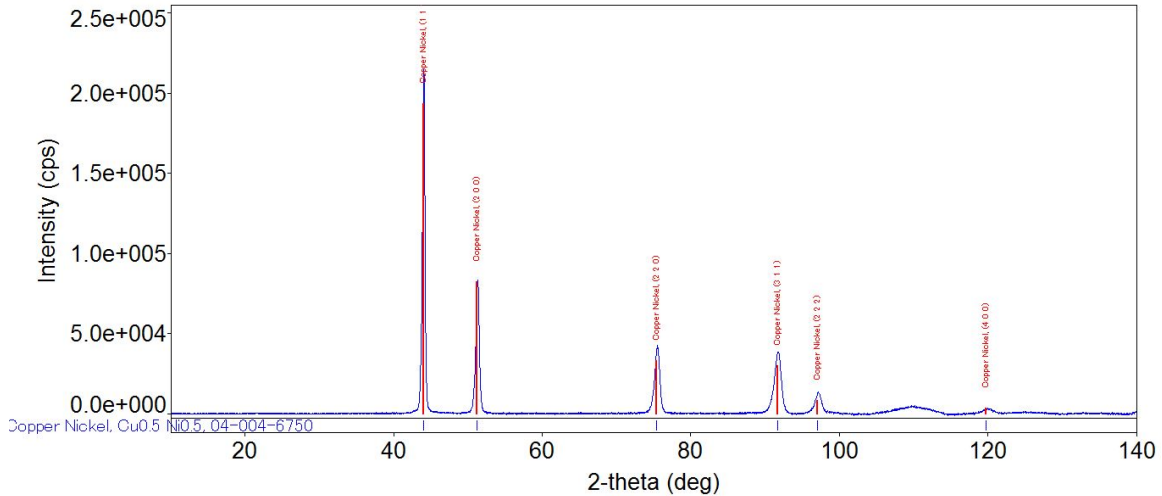
Figure 35.   X-ray Diffraction Pattern for Cu(nano) Ni(nano) HIP
Sample

G.   HARDNESS TESTING

Hardness tests were conducted on the HIP samples to determine the effects of the sintering process and porosity as it relates to the hardness of the CuNi alloy at various temperatures and pressures. The hardness of the Cu(nano) and Ni(nano) was 11.2 HV converted by the Miniflex 600 program. Typical hardness for pure copper is 37 HV (369 MPa) while pure nickel is 65 HV (638 MPA) [19]. Hardness values for CuNi alloys was depended on the nickel content and varied from 90–110 HV [20]. The low hardness is attributed to the high porosity in the sample.
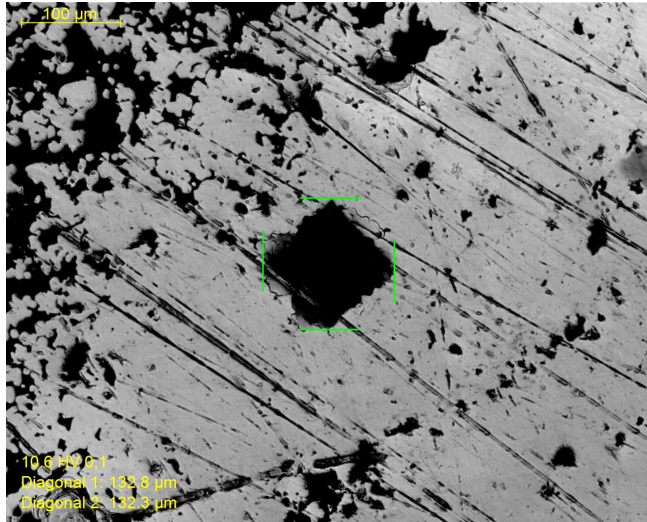
Figure 36.   Cu(nano) Ni(nano) Sample HIP 138 Mpa at 1000°C

Results for Cu (nano) Ni (micro) are shown below in Figure 37 with an average Vickers hardness of 35.36. The lowest Vickers hardness recorded was 22.8 and the highest was 51.4. The varying levels of hardness was a result of the inconsistent porosity in the sample seen in Figure 37.

Specimen Ni(Nano)-Cu(Nano) HIP 20ksi 1000°C	Measurement	Hardness	Method
Specimen 100	Vickers	25.8	HV 0,05
Specimen 101	Vickers	39.5	HV 0,05
Specimen 102	Vickers	45.7	HV 0,05
Specimen 103	Vickers	22.8	HV 0,05
Specimen 104	Vickers	27.7	HV 0,05
Specimen 105	Vickers	30	HV 0,05
Specimen 106	Vickers	21.7	HV 0,05
Specimen 107	Vickers	41.7	HV 0,05
Specimen 108	Vickers	47.3	HV 0,05
Specimen 109	Vickers	51.4	HV 0,05
Average:		35.36	

Figure 37.   Sample 3 Cu(nano) Ni(micro) HIP at 138 Mpa and 1000°C
Hardness Test

44

The hardness of the micron-sized particles had the highest average hardness of HV 99.78. The higher hardness is attributed to the longer sintering temperature and high pressure of 207 Mpa.

Specimen	Measurement	HRC	Method
Specimen 131	Vickers	83.6	HV 0,05
Specimen 131	Vickers	92.7	HV 0,05
Specimen 131	Vickers	88.6	HV 0,05
Specimen 131	Vickers	111	HV 0,05
Specimen 131	Vickers	123	HV 0,05
Average:		99.78	
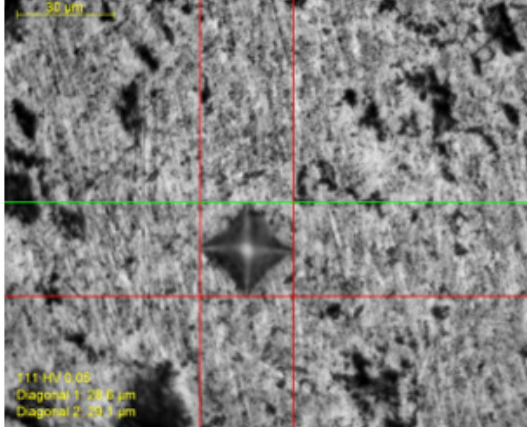
Figure 38.   Sample 8 Cu(micro) Ni(micro) HIP @ 207 Mpa Hardness Test

H.   Summary of Milestones

The following is a list of milestones accomplished by this research:

A suitable binding agent, water/ethanol based gel, was chosen to produce the initial paste to be 3D printed. The gel was easily mixed with metal micro and nanopowders for an extrusion printer.

Several difficulties were found while printing pastes containing nanoparticles. However, based on the paste flow in response to applied forces, measured with a rheometer, the cause of the paste separation was found; nanoparticles in cross-linked gels behave as thinning agents. This discovery led to the determination of micron particles being the ideal material for paste creation with the alcohol gel as a binding agent for extrusion printing.

Then the ideal printing conditions for the metal powder paste were found through trial and error. The printed materials were characterized and found to have no oxidation or changes to the chemical composition of the alloy as a result of binding agent and post-treatment processes.

HIP treatment successfully reduced porosity and increased hardness of the alloy to levels of known CuNi alloys. The measured hardness valued of the cupronickel alloy was 170% greater than pure copper and within the range of other Cu-Ni alloys created through casting methods [19].

IV. CONCLUSION

This final chapter summarizes the findings of this study from the fabrication to the characterization and testing of the final 3D printed products. This chapter also discusses future work that could be explored to improve the technique.

A. ACHIEVEMENTS

This study successfully demonstrated that metal powders could be mixed with binding agents and 3D printed using extrusion printing. The study also showed that the powder mixture can be heat treated to create a copper-nickel alloy with mechanical robustness and desirable microstructure. It was confirmed that heat treatment of the specimens required inert gas to prevent oxidation and other reactions with the raw powders during the sintering process. HIP treatment allowed the porosity to be further decreased and to increase the hardness of the alloy. Hot isostatic treatments of the samples showed even shrinkage, specimens were reduced in size evenly in the x, y, z directions. The specimen's decrease in size during the heat treatment process could be accounted for by increasing the size of the initial print.

The minimum amount of metal powder to binding agent ratio was 46–54% by weight for the S3ed 3D paste printer. Larger printer nozzles could be used which would permit lower ratios of binding agent, but compromise the quality of the print and therefore were not used. The gel chosen was able to be completely removed from the sample without leaving residue or oxidation through heat treatment. As the percentage of binding agent decreased, the porosity of the sample also decreased. Lower porosity samples had higher density, and therefore higher hardness. The Ni(micro) and Cu(micro) powder mixture yielded lower porosity and higher toughness than that of Ni(nano) and Cu(nano). This result is attributed to the viscosity of nanopowder mixtures, which required higher gel content to successfully print. The nanopowder acted as a thinning agent at higher shear rates which caused separation of the mixture while printing.

This study proved that powder metallurgy is possible using 3D printing to create a metal alloy that with promising characteristics for shipboard applications. The smaller

printers and low cost materials used demonstrated that the process can be utilized by the Navy for non-critical applications in the near-term.

B. FUTURE WORK

This research successfully produced a copper-nickel alloy, but there is still room for improvement, research and testing. The first recommendation is to further reduce the porosity of the samples by improving the printing process. Larger ratios of powder-to-gel are possible by using different methods of 3D printing such as vibrating nozzle printers [21]. Porosity can also be improved by exploring heat treatment methods. Pre-sintering of the material before being HIP has shown in other studies to further reduce porosity in powder-metal samples. Larger samples or shipboard parts could also be produced to show proof-of-concept and areas of applicability.

A 50–50% by atomic weight ratio of copper and nickel was used in this study. Different percentages of the metal powders or even addition other metals such as manganese, iron, titanium, or chromium could be changed to improve material characteristics of the alloy. Manganese and iron could improve the strength of the alloy while titanium and chromium may improve corrosion resistance.

Further studies of the copper-nickel alloy such as conducting tensile testing needs to be conducted. Understanding the yield and tensile strength of the alloy as a function of the porosity would show the range of applications the parts could be used for. Other testing such as corrosion resistance and conductivity would also broaden the applications of this research.

Lastly, this research has shown the possibility and applicability of powder metallurgy onboard Navy ships. Cost estimations need to be conducted to determine how this method can be implemented and how much money could be saved with its implementation for the future of a self-sufficient Navy.

LIST OF REFERENCES

[1]   B. Baker, "Made to measure: The next generation of military 3D printing," *Army Technology*, January 23, 2018. [Online]. Available: https://www.army-technology.com/features/made-measure-next-generation-military-3d-printing/

[2]   J. Needham, L. Wang, G. Lu, T. Tsien, D. Kuhn, P. Golas, *Magisteries of Gold and* Immortality (Science and Civilization in China 5)*.* Cambridge, UK: Cambridge University Press, 1974, pp 237-250.

[3]   I. McNeil, *Encyclopedia of the History of Technology.* Ney York, NY, USA: Routledge, 2002.

[4]   V. Bhavar, K. Prakash, P. Vinaykumar, K. Shreyans, K. Gujar, and R. Singh, "A review on powder bed fusion technology of metal additive manufacturing," in *4th International Conference and Exhibition on Additive Manufacturing Technologies*, 2014. [Online] Available: https://www.researchgate.net/profile/Valmik_Bhavar2/publication/285982651_A_review_on_powder_bed_fusion_technology_of_metal_additive_manufacturing/links/570f25de08aed4bec6fdf38d/A-review-on-powder-bed-fusion-technology-of-metal-additive-manufacturing.pdf

[5]   H. Sanchez, C. Du, "Fabrication of 3D printed metal structures by use of high-viscosity Cu paste and a screw extruder," *Journal of Electronic Material*, vol. 44, no. 4, March 2015 [Online] Available: https://doi.org/10.1007/s11664-014-3601-8

[6]   A. Kumar, Y Bai, A. Eklund, C. Williams, "Effects of hot isostatic pressing on copper parts fabricated via binder jetting," *Journal of Procedia Manufacturing*, vol. 10, 2017. [Online] Available: https://www.sciencedirect.com/science/article/pii/S2351978917302664

[7]   A. Zadi-Maad, "The development of additive manufacturing technique for nickel-based alloys: A review," in *AIP Conference Proceedings,* March 2018. [Online] Available: https://www.researchgate.net/publication/320336412_The_development_of_additive_manufacturing_technique_for_nickel-base_alloys_A_review

[8]   F. Anantachaisilp, "Fabrication of shape memory alloys using affordable additive manufacturing routes," M.S. thesis, Dept. of Mech. Eng. NPS, Monterey, CA, USA, 2018.

[9]   Copper Development Association Inc., "Copper-nickel alloys: properties, processing, applications." Accessed April 05, 2019. [Online] Available: https://www.copper.org/applications/marine/cuni/properties/DKI_booklet.html

[10]   International Program on Chemical Safety, "Petroleum, vaseline, paraffin jelly." Accessed April 5, 2019. [Online] Available: http://www.inchem.org/documents/icsc/icsc/eics1440.htm

[11]   ASTM International, "Standard test methods for tension testing of metallic materials." Accessed December 10, 2018. [Online] Available: https://www.astm.org/Standards/E8

[12]   W. Callister, *Material Science and Engineering*. New York, NY, USA: John Wiley and Sons, 2013.

[13]   W. Rasband, MD, USA. 1997. ImageJ, ver. 1.52. [Online]. Available: https://imagej.nih.gov/ij/docs/index.html

[14]   A. Gaharwar, R. Avery, A. Assman, A. Paul, G. McKinley, B. Olsen, "Shear-thinning nanocomposite hydrogels for the treatment of hemorrhage," *ACS Nano,* vol. 8 no. 10, September 2014. [Online]. Available: https://pubs.acs.org/doi/abs/10.1021/nn503719n

[15]   N. Mcintyre, T. Rummery, M. Cook, D. Owen, "X-ray photoelectron spectroscopic study of the aqueous oxidation of Monel-400," *Journal of The Electrochemical Society*, vol. 123, pg.1164-1170, August 1976. [Online]. Available: https://www.researchgate.net/publication/234901917_X-Ray_Photoelectron_Spectroscopic_Study_of_the_Aqueous_Oxidation_of_Monel-400

[16]   D. Herzog, V. Seyda, E. Wycisk, C. Emmelmann, "Additive manufacturing of metals," *Institute of Laser System and Technology*, vol. 177, pg. 371, July 2016. [Online]. Available: https://torpedo.nrl.navy.mil/tu/ps/doc.html?vol=117&dsn=16659648&ssn=17&iss=C&st=JRNAL

[17]   R. Jumaidin, M. Syafiq, M. Hafidzal, M. Zakaria, Mohamad Shukri, "Effect of cooling rate on microstructures and mechanical properties of C102 copper alloy," *Journal of Mechanical Engineering and Technology*, vol. 6, no. 1, January 2014. [Online]. Available: https://www.researchgate.net/publication/268130401_EFFECT_OF_COOLING_RATE_ON_MICROSTRUCTURES_AND_MECHANICAL_PROPERTIES_OF_C102_COPPER_ALLOY

[18]   V. T. Pham, H. T. Bui, B. T. Tran, V. T. Nguyen, D. Quang Le, X. T. Than, V. C. Nguyen, D. P. Doan and Ngoc Minh Phan, "The effect of sintering temperature on the mechanical properties of a Cu/CNT nanocomposite prepared via a powder metallurgy method," *Vietnam Academy of Science & Technology*, vol. 2, no. 1, March 2011. [Online]. Available: https://iopscience.iop.org/article/10.1088/2043-6262/2/1/015006

[19]   Wolfram, "Vickers hardness of the elements." Accessed December 10, 2018. [Online] Available: https://periodictable.com/Properties/A/VickersHardness.v.log.html

[20]   Copper Development Association Inc., "Copper-nickel alloys: mechanical properties." Accessed April 05, 2019. [Online] Available: https://www.copper.org/applications/marine/cuni/properties/mechanical/

[21]   I. Gunduz, "3D printing of extremely viscous materials using ultrasonic vibrations," *Additive Manufacturing*, vol. 22. August 2018. [Online] Available: https://www.sciencedirect.com/science/article/pii/S2214860418301945?via%3Dihub

THIS PAGE INTENTIONALLY LEFT BLANK

INITIAL DISTRIBUTION LIST

1.   Defense Technical Information Center
        Ft. Belvoir, Virginia

2.   Dudley Knox Library
        Naval Postgraduate School
        Monterey, California